Research Square

Preprints are preliminary reports that have not undergone peer review.
They should not be considered conclusive, used to inform clinical practice,
or referenced by the media as validated information.

Two-step hydrothermal method for morphology modulation of barium titanate nanofibers for catalytic dye degradation

Shihao Zhang
Shaanxi Normal University
Wenyuan Gu
Shaanxi Normal University
Juanjuan Wang
Xi'an University of Technology
Zhanhui Peng
Shaanxi Normal University
Qizhen Chai
Shaanxi Normal University
Yuanhao Wang
Shaanxi Normal University
Di Wu
Shaanxi Normal University
Lingling Wei
Shaanxi Normal University
Pengfei Liang
Shaanxi Normal University
Zupei Yang
Shaanxi Normal University
Xiaolian Chao
chaoxl@snnu.edu.cn
Shaanxi Normal University

Research Article

Keywords:

Posted Date: November 18th, 2026

DOI: https://doi.org/10.21203/rs.3.rs-11427421/v1

License: This work is licensed under a Creative Commons Attribution 4.0 International License.
Read Full License

Additional Declarations: No competing interests reported.

Two-step hydrothermal method for morphology modulation of barium titanate nanofibers for catalytic dye degradation

Shihao Zhang[1, #], Wenyuan Gu[1, #], Juanjuan Wang[2,*], Zhanhui Peng[1, *], Qizhen Chai[1], Yuanhao Wang[1], Di Wu[1], Lingling Wei[1], Pengfei Liang[1], Zupei Yang[1, *], Xiaolian Chao[1, *]

[1]Key Laboratory for Macromolecular Science of Shaanxi Province, Shaanxi Key Laboratory for Advanced Energy Devices, Shaanxi Engineering Laboratory for Advanced Energy Technology, School of Materials Science and Engineering, Shaanxi Normal University, Xi'an, 710062, Shaanxi, China;

[2]School of Materials Science and Engineering, Xi'an University of Technology, 710048 Xi'an, China

Co-first author: Shihao Zhang[1, #]; Wenyuan Gu[1, #]

* Corresponding authors:

E-mail addresses: juanwang@xaut.edu.cn (J. W.); yangzp@snnu.edu.cn (Z. Yang), chaoxl@snnu.edu.cn (X. Chao)

Abstract

In this work, $BaTiO_3$ nanofibers were successfully prepared by a two-step hydrothermal method using TiO_2 as the titanium source. In the first step, $Na_2Ti_3O_7$ was synthesized under strong alkaline conditions. It was then converted into $H_2Ti_3O_7$ nanofibers by acid exchange. The results show that the temperature in the first hydrothermal step, from 180 to 240 °C, has a significant effect on the precursor morphology. The $H_2Ti_3O_7$ prepared at 200 °C exhibit the highest aspect ratio and fiber structure. In the second hydrothermal step, this precursor was used as a template. The effects of reaction temperature and time on the morphology and phase were systematically studied. The results show that $BaTiO_3$ nanofibers with the best morphology and uniform structure can be obtained at 210 °C for 85 min. Deviation from this condition leads to damage of the fiber structure and increased particle formation. XRD and Raman results confirm that all samples are tetragonal $BaTiO_3$. The reaction conditions mainly affect the morphology rather than the phase structure. Based on TEM analysis, the formation mechanism is attributed to ion exchange induced by the morphology template of the precursor. This work provides guidance for the optimization of $BaTiO_3$ nanofiber synthesis and improves the understanding of the formation mechanism.

Keywords: Barium titanate, Nanofibers, Precursor, Two-step hydrothermal method

1. Introduction

$BaTiO_3$ is a typical perovskite ABO_3 ferroelectric material. It shows ferroelectric, piezoelectric, and pyroelectric effects[1, 2]. It also has a high dielectric constant. These properties make it important for devices such as capacitors and transducers[3]. Previous studies show that $BaTiO_3$ remains a key material for multilayer ceramic capacitors under the trend of device miniaturization[4, 5]. Its high tetragonality and controllable microstructure are critical for its performance[6, 7].

In recent years, many studies have reported the applications of one dimensional $BaTiO_3$ in different fields[8-11]. Jian et al. filled $BaTiO_3$ nanowires into PVDF and obtained nanocomposite capacitors with high energy density[12]. Zhang et al. found that the dielectric constant and energy storage density increase with the aspect ratio of $BaTiO_3$ nanofibers and their volume fraction in P(VDF-HFP)[13]. Jin et al. used $BaTiO_3$ nanowires to degrade organic pollutants in wastewater, and the degradation efficiency reached up to 95%[14]. Compared with particle morphology, one dimensional nanofibers have a higher aspect ratio. They are more likely to deform under external disturbance. This leads to a higher piezoelectric potential. Wu et al. confirmed this result through experiments and finite element method simulations[15].

At present, the two-step hydrothermal method is widely used to prepare $BaTiO_3$ nanofibers[7, 16, 17]. A direct one step hydrothermal process usually produces particle morphology. It is difficult to obtain well defined one dimensional $BaTiO_3$ structures without assistance. The formation of one dimensional structures often requires templates, specific precursors, or ion exchange routes[18-20]. Many studies show that layered titanates with one dimensional structures have open interlayer spaces[21-23]. These structures provide good ion exchange ability and topological transformation potential. They are important precursors for the preparation of one dimensional $BaTiO_3$. Hu et al. synthesized one dimensional $BaTiO_3$ using $H_2Ti_4O_9 \cdot H_2O$ as a precursor[22]. Some studies report that $Na_2Ti_3O_7$ has better ion exchange ability than other sodium titanates with different stoichiometries. After acid treatment, about 94% of Na^+ ions can be replaced by H^+ ions[24]. Therefore, most researchers use $H_2Ti_3O_7$ nanofibers as precursors to synthesize $BaTiO_3$ nanofibers[17, 24, 25]. In this work, $BaTiO_3$ nanofibers were fabricated via a two-step hydrothermal method. The optimal synthesis conditions for nanofiber production were explored, and the

underlying formation mechanism of $BaTiO_3$ nanofibers was analyzed. This study provides certain references for the preparation of barium titanate nanofibers.

2. Experimental Section

In the first hydrothermal step, TiO_2 and NaOH are used as reactants. 48 g of NaOH powder and 2.5 g of TiO_2 powder are mixed in 120 mL of deionized water. The mixture is then transferred into a 200 mL Teflon lined autoclave and sealed. It is heated at 180 to 240 °C for 24 h. After the reaction, the system cools naturally to room temperature. The white product is collected by centrifugation and washed with deionized water until neutral. The obtained white product is $Na_2Ti_3O_7$ nanofibers. The white product is then mixed with 0.2 mol per liter hydrochloric acid solution and stirred for 4 h to ensure a complete reaction. After the reaction, the product is collected by centrifugation and washed with deionized water until neutral. It is dried at 70 °C for 24 h to obtain the intermediate product $H_2Ti_3O_7$ nanofibers. In the second hydrothermal step, the intermediate $H_2Ti_3O_7$ nanofibers and $Ba(OH)_2{\cdot}8H_2O$ are used to prepare $BaTiO_3$ nanofibers. 0.2580 g of $H_2Ti_3O_7$ powder and 1.8928 g of $Ba(OH)_2{\cdot}8H_2O$ powder are mixed in 120 mL of deionized water. The mixture is then transferred into a 200 mL Teflon lined autoclave and sealed. It is heated at 180 to 240 °C for 60 to 110 min. After the reaction, the system cools naturally to room temperature. The white product is collected by centrifugation and washed with deionized water until neutral. It is dried at 70 °C for 24 h to obtain the final product $BaTiO_3$ nanofibers[15, 17, 24].

In this work, the parameters of the first and second hydrothermal steps were adjusted to prepare $BaTiO_3$ nanofibers. First, $H_2Ti_3O_7$ nanofibers were synthesized at different temperatures in the first hydrothermal step, including 180, 200, 220, and 240 °C. These precursors were then converted into $BaTiO_3$ under fixed conditions in the second hydrothermal step at 210 °C for 85 min. Second, $H_2Ti_3O_7$ prepared at 200 °C was used as the precursor. In the second hydrothermal step, the temperature was fixed at 210 °C while the reaction time was varied as 60, 85, and 110 min. In addition, the reaction time was fixed at 85 min while the temperature was varied as 180, 210, and 240 °C to synthesize $BaTiO_3$ nanofibers.

The obtained samples were characterized by several techniques. These include X-ray diffraction (XRD, Mini Flex-600), Raman spectroscopy (Raman, inVia Reflex), transmission

electron microscopy (TEM, JEM-2800), and scanning electron microscopy (SEM, SU8020). Energy dispersive spectroscopy (EDS, X-MAX80) was also used together with SEM.

3. Results and Discussion

Figure 1 shows the SEM images of the precursor $H_2Ti_3O_7$ nanofibers. The samples synthesized at 180 °C, 200 °C, 220 °C, and 240 °C all exhibit a one dimensional nanofiber morphology. The samples prepared at 180 °C, 200 °C, and 220 °C show a relatively high aspect ratio. Figure 2 shows the SEM images of $BaTiO_3$ nanofibers synthesized by the second hydrothermal step using $H_2Ti_3O_7$ nanofibers prepared at different temperatures as precursors. The morphology of the obtained $BaTiO_3$ products shows a good correspondence with that of the $H_2Ti_3O_7$ precursors. As shown in Table 1, the average aspect ratios of the $H_2Ti_3O_7$ precursors and the $BaTiO_3$ products were calculated. The results show that the change in aspect ratio of the $BaTiO_3$ fibers with synthesis temperature follows the same trend as that of the precursor fibers. These results suggest that $H_2Ti_3O_7$ nanofibers act as a morphology template during the second hydrothermal process. This template effect induces the formation of $BaTiO_3$ in a fibrous structure.

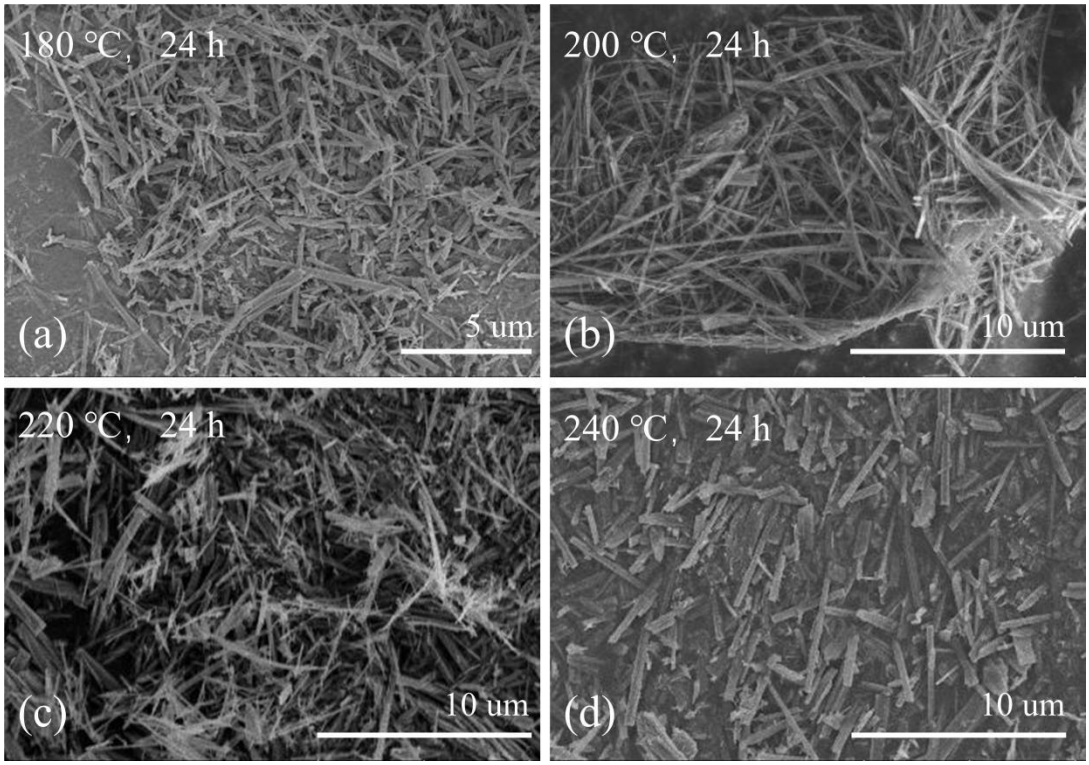


Figure 1 SEM images of $H_2Ti_3O_7$ samples synthesized at different temperatures: (a) 180 °C; (b) 200 °C; (c) 220 °C; (d) 240 °C

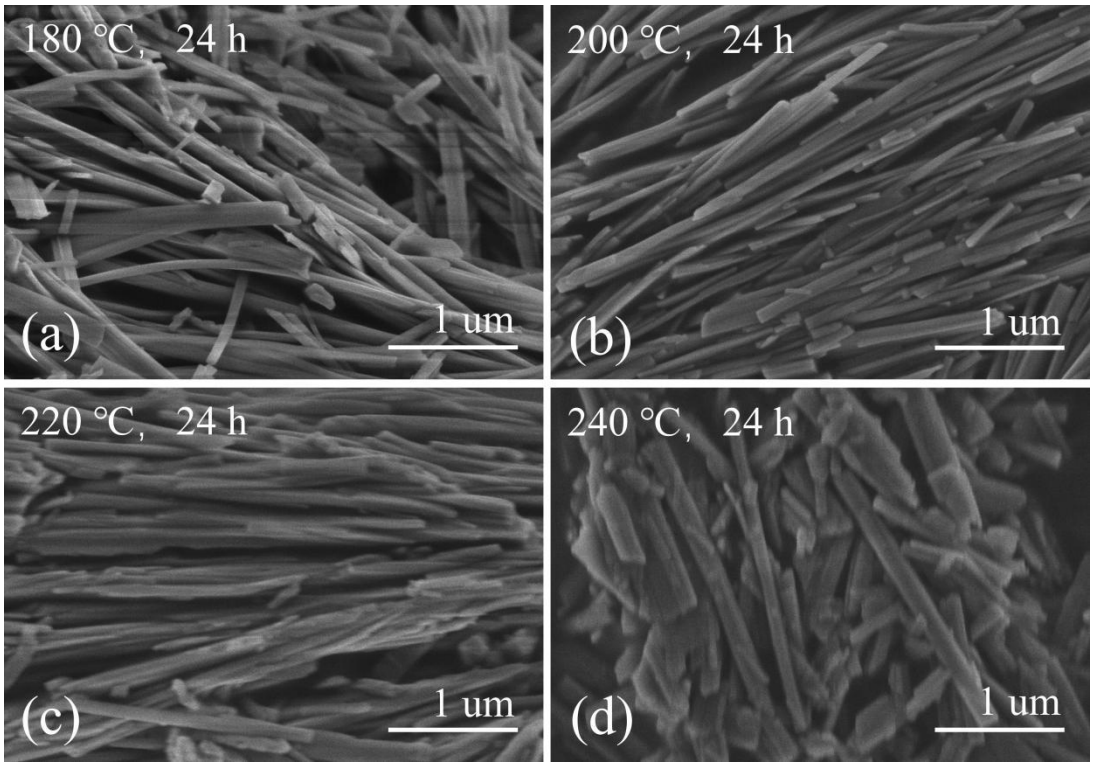


Figure 2 SEM images of $BaTiO_3$ samples prepared from $H_2Ti_3O_7$ nanofibers synthesized at different temperatures: (a) 180 °C; (b) 200 °C; (c) 220 °C; (d) 240 °C

Table 1 Average aspect ratio of precursor and product fibers synthesized at different temperatures

Samples	180 °C	200 °C	220 °C	240 °C
$H_2Ti_3O_7$	20	33	16	11
$BaTiO_3$	18	27	13	6

To further confirm the chemical composition and elemental distribution of the prepared products, EDS analysis was performed on a single $BaTiO_3$ nanofiber. The results are shown in Figure 3. The spectrum shows that the $BaTiO_3$ nanofiber contains only Ba, Ti, and O elements. No characteristic peaks of impurity elements are detected. The elemental mapping images show that Ba, Ti, and O are uniformly distributed within the nanofiber. No obvious element enrichment is observed. These results indicate that the prepared $BaTiO_3$ nanofibers have high compositional uniformity and no significant impurities are introduced during the synthesis process.

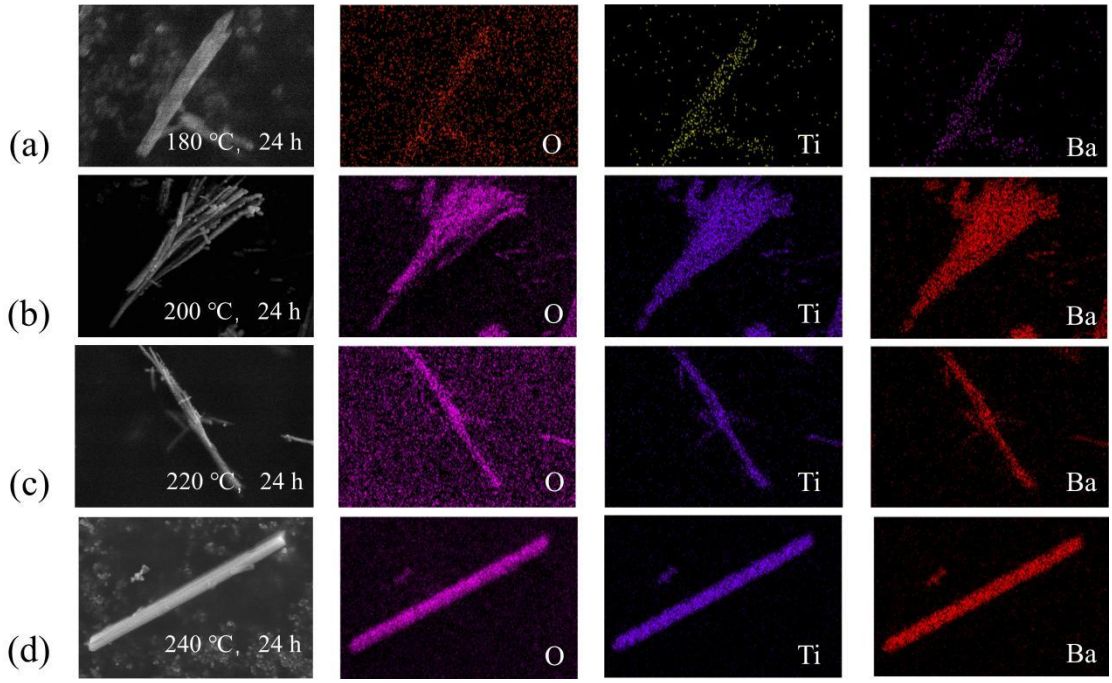


Figure 3 EDS spectra of $BaTiO_3$ samples prepared from $H_2Ti_3O_7$ nanofibers synthesized at different temperatures: (a) 180 °C; (b) 200 °C; (c) 220 °C; (d) 240 °C

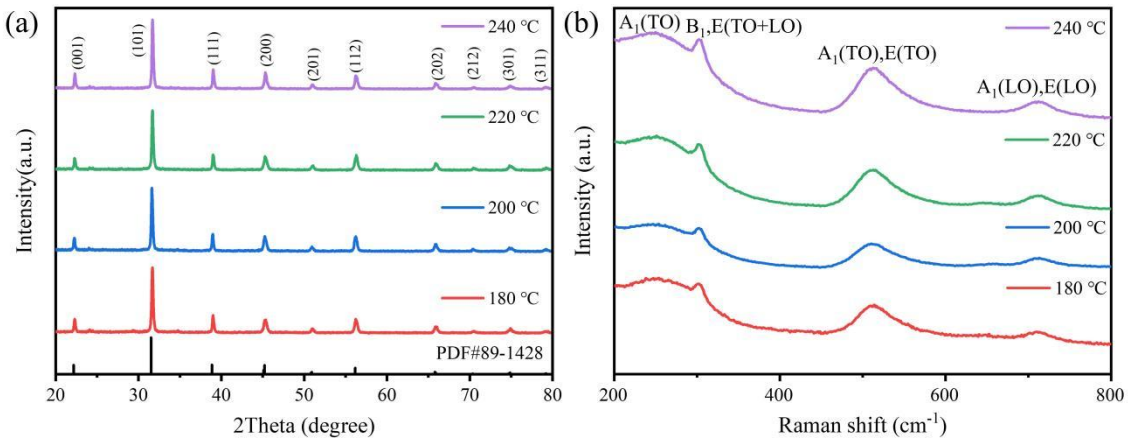


Figure 4 (a) XRD patterns and (b) Raman spectra of $BaTiO_3$ samples prepared from $H_2Ti_3O_7$ nanofibers synthesized at different temperatures

Figure 4(a) shows the XRD patterns of $BaTiO_3$ nanofibers synthesized using $H_2Ti_3O_7$ precursors prepared at different temperatures. The diffraction peaks of all samples match well with the standard card of $BaTiO_3$ (PDF#89-1428). No obvious impurity peaks are observed. This result indicates that all samples form a tetragonal perovskite structure. Figure 4(b) shows the corresponding Raman spectra. The main characteristic peaks appear at about 246 cm^{-1}, 303 cm^{-1}, 512 cm^{-1}, and 712 cm^{-1}. The peak at about 246 cm^{-1} is a broad peak and corresponds to A1(TO).

The peak at about 303 cm^{-1} is a sharp peak and corresponds to B1 and E(TO+LO). The peak at about 512 cm^{-1} is a broad peak and corresponds to A1(TO) and E(TO). The peak at about 712 cm^{-1} is a broad peak and corresponds to A1(LO) and E(LO)[14, 15, 17]. These characteristic peaks are consistent with the vibration modes of tetragonal $BaTiO_3$. This result further confirms the tetragonal perovskite structure indicated by XRD. Based on the morphology and phase structure results, the $H_2Ti_3O_7$ nanofibers prepared at 200 °C were selected as the precursor. The product fibers from this precursor show well maintained morphology and clear structure. These samples are used for further study of the effect of the second hydrothermal conditions on the formation of $BaTiO_3$ nanofibers.

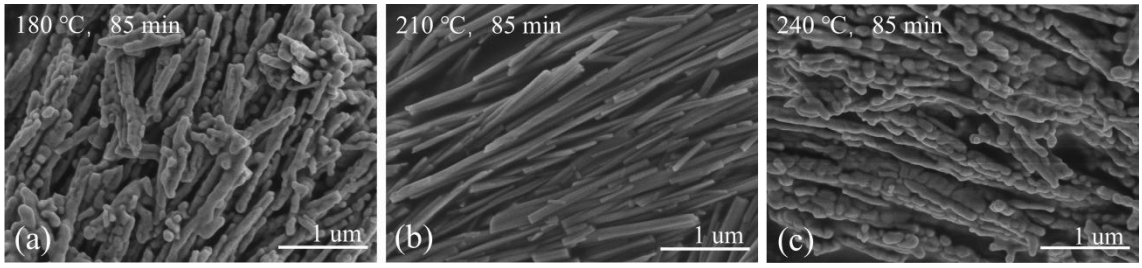


Figure 5 SEM images of $BaTiO_3$ samples prepared at different temperatures using $H_2Ti_3O_7$ precursor synthesized at 200 °C: (a) 180 °C; (b) 210 °C; (c) 240 °C

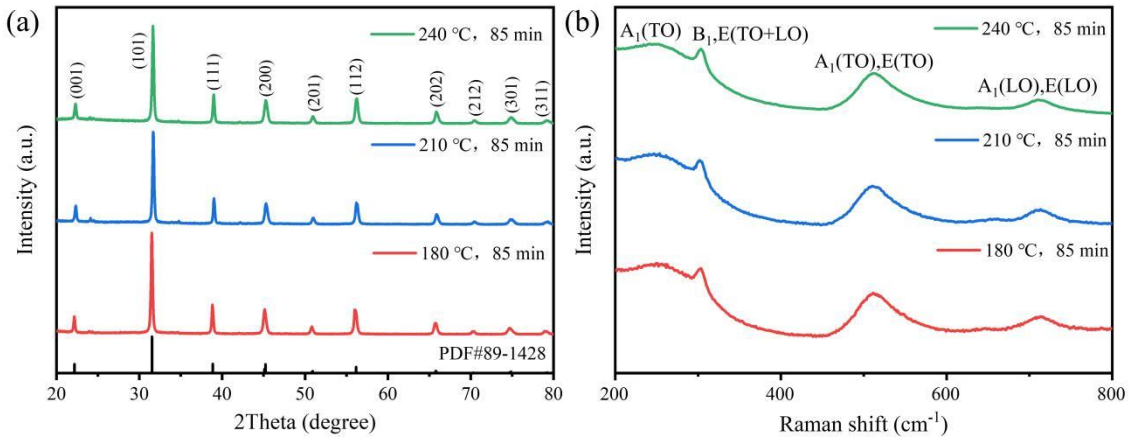


Figure 6 (a) XRD patterns and (b) Raman spectra of $BaTiO_3$ samples prepared at different temperatures using $H_2Ti_3O_7$ precursor synthesized at 200 °C

In the second hydrothermal step, the reaction temperature was first adjusted. Based on 210 °C, two additional temperatures of 180 °C and 240 °C were set. The microstructures of the obtained samples are shown in Figure 5. When the reaction temperature decreases or increases, the fibrous morphology becomes less pronounced. When the temperature increases to 240 °C,

obvious particle formation appears. The fiber structure is seriously damaged. Figure 6 shows the XRD patterns and Raman spectra of the corresponding samples. All XRD patterns match well with the standard card of $BaTiO_3$ (PDF#89-1428). No obvious impurity peaks are observed. The Raman spectra show the typical features of tetragonal $BaTiO_3$. These results indicate that the phase structure remains stable within this temperature range. The temperature mainly affects the morphology retention rather than the phase composition.。

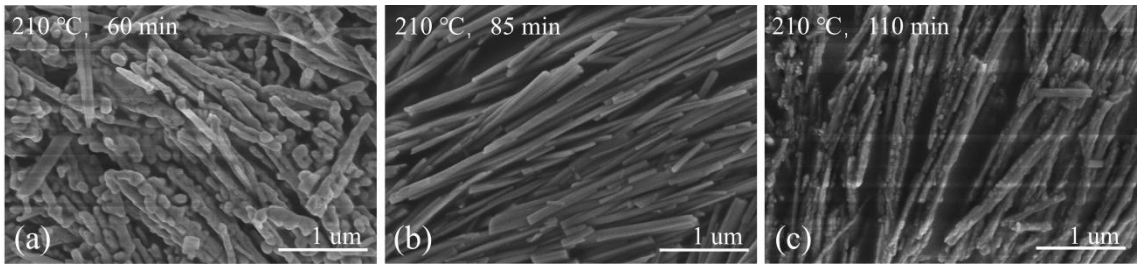


Figure 7 SEM images of $BaTiO_3$ samples prepared with different reaction times using $H_2Ti_3O_7$ precursor synthesized at 200 °C: (a) 60 min; (b) 85 min; (c) 110 min

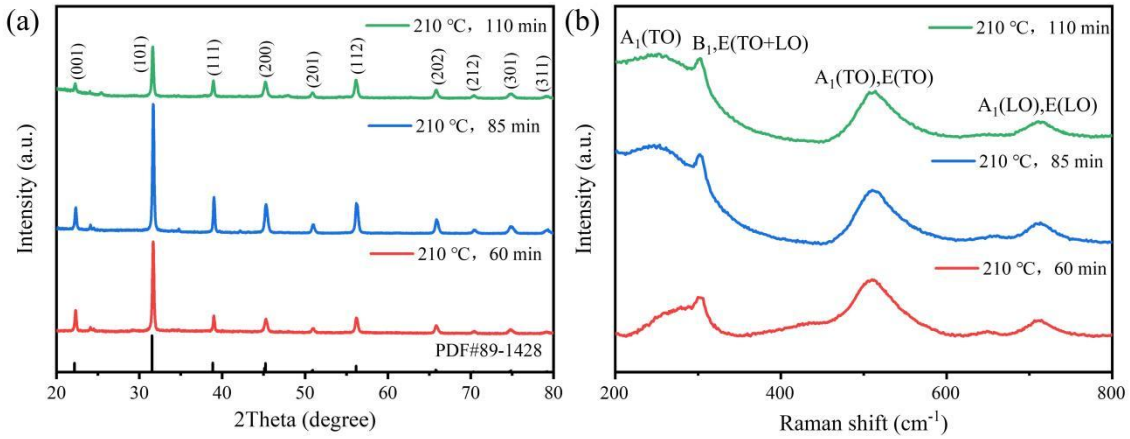


Figure 8 (a) XRD patterns and (b) Raman spectra of $BaTiO_3$ samples prepared with different reaction times using $H_2Ti_3O_7$ precursor synthesized at 200 °C

Then, with the reaction temperature fixed at 210 °C, the reaction time in the second hydrothermal step was further adjusted. Based on 85 min, two comparison times of 60 min and 110 min were set. The morphologies of the obtained samples are shown in Figure 7. When the reaction time is shortened, the fibrous morphology decreases. This result indicates that an insufficient reaction degree makes it difficult to fully transform or stabilize the fiber structure. When the reaction time is extended to 110 min, the sample still maintains a certain fibrous morphology. However, the overall morphology and uniformity are inferior to those of the sample

prepared at 85 min. The XRD patterns and Raman spectra shown in Figure 8 further confirm that all samples obtained at different reaction times match well with the tetragonal $BaTiO_3$ structure (PDF#89-1428). No obvious impurity phases are observed. These results indicate that the change in reaction time mainly affects the morphology evolution and fiber retention, while it has little influence on the crystal phase.

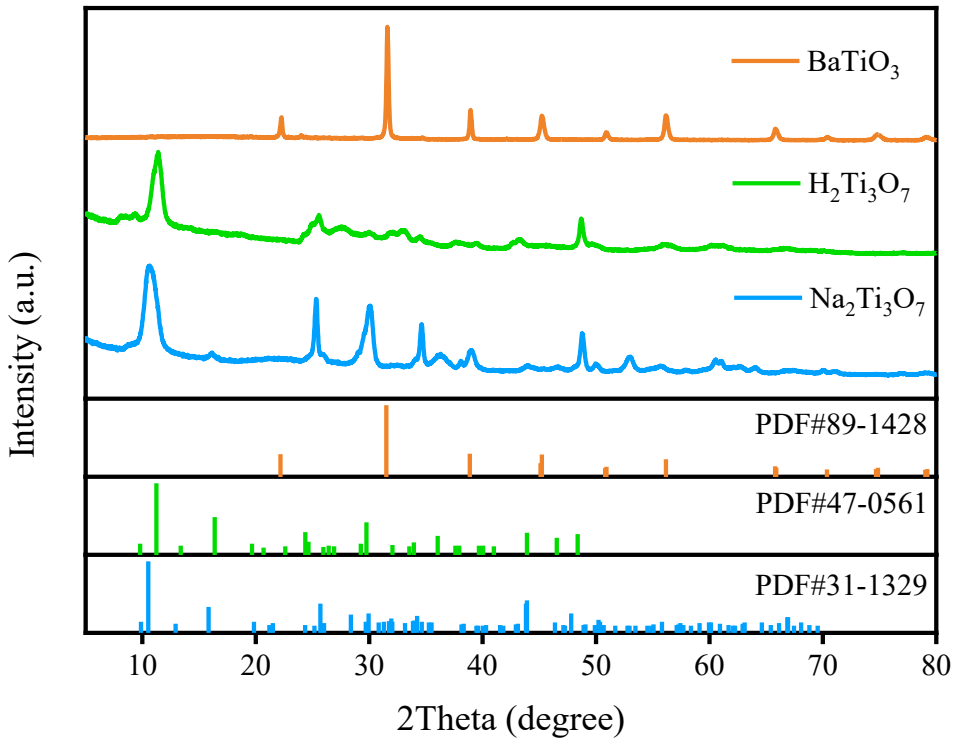


Figure 9 XRD patterns of $Na_2Ti_3O_7$, $H_2Ti_3O_7$, and $BaTiO_3$

To explore the possible formation mechanism of $BaTiO_3$ nanofibers, the morphology and structure of the precursors and products were characterized. Figure 9 shows the XRD patterns of $Na_2Ti_3O_7$, $H_2Ti_3O_7$, and $BaTiO_3$, together with the corresponding PDF cards. $Na_2Ti_3O_7$ matches well with PDF#31-1329. $H_2Ti_3O_7$ matches well with PDF#47-0561. $BaTiO_3$ matches well with PDF#89-1428. The XRD pattern of $H_2Ti_3O_7$ is clearly different from that of $Na_2Ti_3O_7$. This result indicates that acid treatment causes a change in phase structure that can be identified by XRD. The differences in peak shape and the matching results indicate a clear phase evolution process of $Na_2Ti_3O_7$ to $H_2Ti_3O_7$ to $BaTiO_3$.

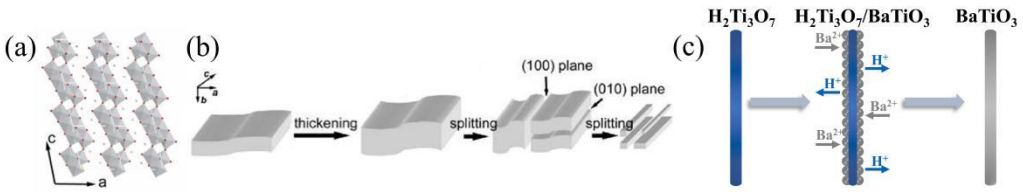


Figure 10 (a) $Na_2Ti_3O_7/H_2Ti_3O_7$ Structural Model; (b) Schematic diagram of the formation process of $Na_2Ti_3O_7$ nanofibers; (c) Schematic diagram of the formation process of $BaTiO_3$ nanofibers by $H_2Ti_3O_7$ nanofibers

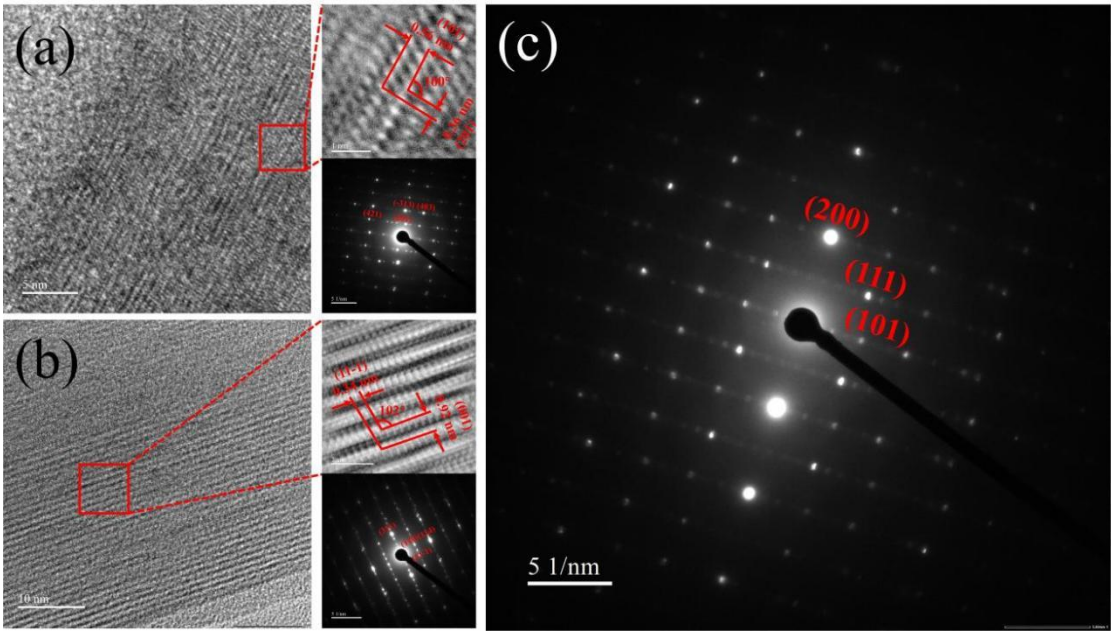


Figure 11 TEM images: (a) $Na_2Ti_3O_7$; (b) $H_2Ti_3O_7$; (c) $BaTiO_3$

Figure 10(a) depicts the layered crystal structures of $Na_2Ti_3O_7$ and $H_2Ti_3O_7$, explicitly indicating the Ti–O octahedral framework and the interlayer exchangeable cations (Na^+/H^+). In turn, the high-resolution TEM images in Figures 11(a) and 11(b) precisely calibrate the periodic dimensions of this structural model through experimentally measured lattice spacings—0.56 nm and 0.36 nm for $Na_2Ti_3O_7$, and 0.92 nm for the (001) planes of $H_2Ti_3O_7$ along with another spacing of 0.34 nm. Critically, the well-resolved layered stacking and the 0.92 nm interlayer spacing observed in Figure 11(b) confirm that the framework does not undergo collapse after acid exchange ($Na^+ \rightarrow H^+$). This finding is in full agreement with the model proposed in Figure 10(a), which assumes only a change in interlayer cations while retaining the layered configuration, thereby providing quantitative lattice data that robustly underpins the structural model.

Figure 10(b) schematically illustrates the self-assembly of TiO_2 into one-dimensional $Na_2Ti_3O_7$ nanofibers via dissolution, rearrangement, and recrystallization under highly alkaline

hydrothermal conditions. In contrast, the TEM images in Figure 11(a) not only clearly reveal a fibrous morphology, but also exhibit regular spots in the selected-area electron diffraction (SAED) pattern, along with continuous and sharp lattice fringes, indicating that the products possess high crystallinity and characteristic unidirectional growth. This experimental evidence irrefutably confirms the oriented-rearrangement nucleation pathway depicted in Figure 10(b), as opposed to random aggregation—if simple precipitation were the dominant process, such a well-defined one-dimensional morphology and single-crystal-like diffraction patterns would be unattainable. Consequently, this provides an accurate elucidation of the mechanism governing morphology formation.

Figure 10(c) illustrates that when Ba^{2+} exchange triggers the rearrangement of the Ti–O framework from a layered to a perovskite structure, the product retains a fibrous morphology (template conversion) if the reaction is confined to the solid–liquid interface and inherits the precursor geometry. Conversely, when the contribution of local dissolution–precipitation increases, isolated particles are generated. The SAED pattern in Figure 11(c) can be indexed to the (101), (111), and (200) diffraction planes of perovskite $BaTiO_3$, confirming the successful phase transformation. Concurrently, the morphology exhibits a mixed state of fibers and particles, which precisely corresponds to the coexistence of the two mechanisms. The document explicitly notes that the reduction in fibrous morphology correlates with changes in reaction conditions, which is an inevitable manifestation of the competitive model depicted in Figure 10(c) as observed in the actual images of Figure 11(c), the residual fibrous regions evidence topological inheritance, while the presence of particles indicates the intervention of dissolution–precipitation. The coexistence of both pathways elevates the phase transformation mechanism from a single speculative assumption to a comprehensive scientific explanation that incorporates multiple thermodynamic routes, thereby fully revealing the essential principles governing the conversion from layered titanates to perovskite.

4. Summary

In summary, $BaTiO_3$ nanofibers were successfully fabricated via a two-step hydrothermal method using TiO_2 as the titanium source, involving the formation of $Na_2Ti_3O_7$ under strong alkaline conditions and its conversion to $H_2Ti_3O_7$ nanofiber precursor by acid exchange. $H_2Ti_3O_7$

exerts a significant morphological template effect on the final product, and the precursor synthesized at 200 °C delivers the highest aspect ratio and intact fibrous structure. The optimal condition for the second hydrothermal step is identified as 210 °C for 85 min; deviations in reaction temperature or duration result in deteriorated fibrous morphology and increased particle formation. XRD and Raman characterizations confirm that all as-prepared samples maintain a tetragonal perovskite structure, revealing that the synthetic parameters predominantly regulate morphology rather than crystal phase. This work offers practical guidance for the controllable preparation of $BaTiO_3$ nanofibers and deepens the understanding of the topological transformation-based formation mechanism of one-dimensional barium titanate nanostructures.

Competing interests

The authors have no competing interests to declare that are relevant to the content of this article.

Acknowledgments

This work was supported by the National Natural Science Foundation -Cultural Relics Joint Foundation of China (Grant No. U2574210)， the authors would also like to thank the Fundamental Research Funds for the Central Universities (Grant Nos. GK202605005), the Key Project on Integrating the “Four Chains” at the Shaanxi Qinchuangyuan Industrial Innovation Cluster Zone (2025CY-JJQ-37).

Availability of data and materials

The data that support the findings of this study are available from the corresponding author upon reasonable request.

References

[1] Chelladurai D, Kohli M, Winiger J, et al. Barium titanate and lithium niobate permittivity and Pockels coefficients from megahertz to sub-terahertz frequencies [J]. *Nature Materials*, **2025**, 24(6): 868-75.

[2] Jiang B, Iocozzia J, Zhao L, et al. Barium titanate at the nanoscale: controlled synthesis and dielectric and ferroelectric properties [J]. *Chemical Society Reviews*, **2019**, 48(4): 1194-228.

[3] Zhang K, Gao P, Liu C, et al. Structural evolution and enhanced piezoelectric activity in novel lead-free $BaTiO_3$-$Ca(Sn_{1/2}Zr_{1/2})O_3$ solid solutions [J]. *Energies*, **2022**, 15(20): 7795.

[4] Kishi H, Mizuno Y, Chazono H. Base-metal electrode-multilayer ceramic capacitors: past, present and future perspectives [J]. *Japanese Journal of Applied Physics*, **2003**, 42(1): 1-15.

[5] Xiao M, Zhen Y, Zhu C, et al. Effect of Ho-Dy co-doping on the electrical properties and reliability of $BaTiO_3$-based nanoceramics for Base Metal Electrode Multilayer Ceramic Capacitor [J]. *Journal of the American Ceramic Society*, **2023**, 106(10): 5898-906.

[6] Luan S, Wang P, Zhang L, et al. Atmospherically hydrothermal assisted solid-state reaction synthesis of ultrafine $BaTiO_3$ powder with high tetragonality [J]. *Journal of Electroceramics*, **2023**, 50(4): 97-111.

[7] Chen S, Han B, Chen X, et al. Hydrothermal synthesis and morphology control mechanism of $BaTiO_3$ from $NaTi_3O_6(OH)(H_2O)_2$ precursors [J]. *Ceramics International*, **2024**, 50(12): 21779-87.

[8] Xue K, Jiang Y, Mofarah SS, et al. Composition-driven morphological evolution of $BaTiO_3$ nanowires for efficient piezocatalytic hydrogen production [J]. *Chemosphere*, **2023**, 338(139337.

[9] Pan Z, Yao L, Zhai J, et al. High-Energy-Density Polymer Nanocomposites Composed of Newly Structured One-Dimensional $BaTiO_3$@Al_2O_3 Nanofibers [J]. *ACS Applied Materials & Interfaces*, **2017**, 9(4): 4024-33.

[10] Wang J, Sun Y, Wang P, et al. High energy density of polyimide composites containing one-dimensional $BaTiO_3$@ZrO_2 nanofibers for energy storage device [J]. *Journal of Alloys and Compounds*, **2019**, 789(785-91.

[11] Wan B, Li H, Xiao Y, et al. Enhanced dielectric and energy storage properties of $BaTiO_3$ nanofiber/polyimide composites by controlling surface defects of $BaTiO_3$ nanofibers [J]. *Applied Surface Science*, **2020**, 501(144243.

[12] Jian G, Jiao Y, Meng Q, et al. Hydrothermal synthesis of $BaTiO_3$ nanowires for high energy density nanocomposite capacitors [J]. *Journal of Materials Science*, **2020**, 55(16): 6903-14.

[13] Zhang D, Zhou X, Roscow J, et al. Significantly enhanced energy storage density by modulating the aspect ratio of $BaTiO_3$ nanofibers [J]. *Scientific Reports*, **2017**, 7(1): 45179.

[14] Jin C, Liu D, Hu J, et al. The role of microstructure in piezocatalytic degradation of organic dye pollutants in wastewater [J]. *Nano Energy*, **2019**, 59(372-9.

[15] Wu J, Qin N, Bao D. Effective enhancement of piezocatalytic activity of $BaTiO_3$ nanowires under ultrasonic vibration [J]. *Nano Energy*, **2018**, 45(44-51.

[16] Cao Y, Zhu K, Wu Q, et al. Hydrothermally synthesized barium titanate nanostructures from $K_2Ti_4O_9$ precursors: Morphology evolution and its growth mechanism [J]. *Materials Research Bulletin*, **2014**, 57(162-9.

[17] Surmenev RA, Chernozem RV, Skirtach AG, et al. Hydrothermal synthesis of barium titanate nano/microrods and particle agglomerates using a sodium titanate precursor [J]. *Ceramics International*, **2021**, 47(7, Part A): 8904-14.

[18] Jeong CK, Baek C, Kingon AI, et al. Lead-Free Perovskite Nanowire-Employed Piezopolymer for Highly Efficient Flexible Nanocomposite Energy Harvester [J]. *Small*, **2018**, 14(19): 1704022.

[19] Bao N, Shen L, Gupta A, et al. Size-controlled one-dimensional monocrystalline $BaTiO_3$

nanostructures [J]. *Applied Physics Letters*, **2009**, 94(25): 253109.

[20] Maxim F, Vilarinho PM, Ferreira P, et al. Kinetic Study of the Static Hydrothermal Synthesis of $BaTiO_3$ Using Titanate Nanotubes Precursors [J]. *Crystal Growth & Design*, **2011**, 11(8): 3358-65.

[21] Wu D, Liu J, Zhao X, et al. Sequence of events for the formation of Titanate nanotubes, nanofibers, nanowires, and nanobelts [J]. *Chemistry of Materials*, **2006**, 18(2): 547-53.

[22] Hu D, Miao L, Zhang Z, et al. One-dimensional piezoelectric $BaTiO_3$ polycrystal of topochemical mesocrystal conversion from layered $H_2Ti_4O_9{\cdot}H_2O$ single crystal [J]. *Crystal Growth & Design*, **2018**, 18(12): 7264-74.

[23] Liu T, Miao L, Yao F, et al. Structure, properties, preparation, and application of layered Titanates [J]. *Inorganic Chemistry*, **2023**, 63(1): 1-26.

[24] Dadashov S, Suvaci E. Optimization of $Na_2Ti_3O_7$ nanowire synthesis conditions for reliable $BaTiO_3$ nanowires production [J]. *Open Ceramics*, **2025**, 23(100827.

[25] Bao N, Shen L, Srinivasan G, et al. Shape-controlled monocrystalline ferroelectric Barium Titanate nanostructures: from nanotubes and nanowires to ordered nanostructures [J]. *The Journal of Physical Chemistry C*, **2008**, 112(23): 8634-42.